Pergamon

PII: S0021-8502(96)00488-0

J. Aerosol Sci., Vol. 28, No. 6, pp. 937–957, 1997

0021–8502/97 $17.00 + 0.00

LIGHT SCATTERING STUDY OF FRACTAL CLUSTER AGGREGATION NEAR THE FREE MOLECULAR REGIME

C. Oh and C.M. Sorensen

Department of Physics, Cardwell Hall, Kansas State University, Manhattan, KS 66506-2601, U.S.A.

(*First received* 4 *September* 1996; *and in final form* 18 *November* 1996)

Abstract—This paper presents light scattering measurements of the aggregation rate for an aerosol of fractal aggregates in a rarefied gas. A premixed ethylene/oxygen flame was used to create a hot, fractal aggregate aerosol of carbonaceous soot. Static light scattering involving absolute scattering, extinction, and optical structure factor measurements was used to measure the soot cluster morphological parameters, cluster radius of gyration, fractal dimension, monomers per aggregate and monomer size, all as a function of height above burner. Laser Doppler velocimetry was used to convert height to time. Above a height of 7 mm, it was established that aggregation was the dominant growth mechanism. The aggregation cluster growth kinetics are compared to the Smoluchowski equation prediction using an aggregation kernel that accounts for the fractal nature of the aggregates. The kinetics of this system ranged from the free molecular to the Epstein regime. Comparison of experiment to theory shows the theory to be from 15 to 100% too low which may be compared to an experimental uncertainty of a factor of two due largely to soot particle refractive index uncertainty. The discrepancy could be due to attractive dispersive forces between aerosol particles. These discrepancies are small, however, compared to the range of the aggregation kernel. Hence this work establishes the validity of the theoretical form of the kernel for fractal aggregates in rarefied gases. © 1997 Elsevier Science Ltd.

INTRODUCTION

Aggregation is the mechanism by which finely divided matter seeks to become whole. The aggregation mechanism occurs in a wide variety of colloidal and aerosol systems with either liquid or solid particles. This wide variety leads to a richness of phenomena. As the suspending fluid rarefies, the aggregation kinetics pass through three different regimes, two involving two types of diffusional motion and one involving ballistic (straight line) motion of the particles (Seinfeld, 1986). Convoluted with these regimes are differences in agglomerate morphology. The morphology can be dense, due to coalescence of liquid-like drops to form larger drops, or nondense, which occurs when solid particles aggregate. In this latter case it is now well established that the aggregates are describable as fractals (Forrest and Witten, 1979; Weitz and Oliveria, 1984; Schaefer *et al.*, 1984; Family and Landau, 1984; Samson *et al.*, 1987; Dobbins and Megaridis, 1987, Zhang *et al.*, 1988). These fractal aggregates are quantified by their fractal dimension D_f, less than the spatial dimension, such that the number of monomers (primary particles) per aggregate scales with the overall aggregate radius as $N \sim R^{D_f}$. It is valuable to quantify this relationship as (Sorensen *et al.*, 1992a)

$$N = k_0(R_g/a)^{D_f} \tag{1}$$

where k_0 is a prefactor, R_g is the cluster radius of gyration, and a is the monomer radius. For aerosols and most colloids $D_f \simeq 1.8$ which is consistent with the concept of Diffusion Limited Cluster Aggregation (DLCA) developed from computer simulations. Recently it has been determined that $k_0 = 1.3 \pm 0.1$ for these DLCA aggregates in three dimensions (Cai *et al.*, 1995; Sorensen and Roberts, 1997; Oh and Sorensen, 1997).

Due to the importance of this phenomenon, aggregation has seen considerable previous work (Mercer, 1976; Bunz, 1990) which has been a mix of the possible kinetics and aggregate morphology described above. The majority of this work has been in the continuum regime,

where the ratio of the suspending fluid molecule mean free path to particle radius, the Knudsen number, Kn, is small, because of its accessibility, e.g. all colloids are in this regime as well as room temperature aerosols of large particles. With the advent of the fractal concept, much work in the physics literature has been concerned with scaling behavior of the colloidal aggregate growth, i.e. the power law dependencies with time, and has taken account of the fractal nature of the aggregates in the scaling (Martin and Schaefer, 1984; Weitz *et al.*, 1984; Olivier and Sorensen, 1990). However, these studies have not made absolute measurements of the aggregation rate. On the other hand, there have been careful quantitative studies of the aggregation rate in both liquid drop (nonfractal) and solid particle (presumably fractal) aerosol systems in both the continuum ($Kn = 0$) and transition regimes ($Kn \sim 1$) (Fuchs and Sutugin, 1965; Wagner and Kerker, 1977; Okuyama *et al.*, 1984, 1986; Kim and Liu, 1984; Szymanski *et al.*, 1989, Olivier *et al.*, 1992). These studies have shown good agreement (10% to a factor of two) between experiment and theory for these regimes. To our knowledge the only studies of aggregation at large Knudsen numbers ($Kn \gg 1$) are those involving soot aerosols in flames (Prado *et al.*, 1981; Puri *et al.*, 1993; Felderman *et al.*, 1994; Jander *et al.*, 1995). Flames allow this possibility because the elevated temperature increases the gas molecule mean free path by a factor of ca. six over room temperature. The previous pioneering efforts have shown qualitative agreement between theory and experiment for the aggregation rate. Lacking in all these previous works, however, is one or more of either proper use of aggregate light scattering principles, comparison to the complete aggregation kernel involving cross over from free molecular to Epstein rather than solely the free molecular kernel, or use of the simple Smoluchowski equation (equation (B10)) rather than the complete equation (equation (2)) with polydispersity. Building on the past we have attempted to perform a complete experiment for fractal aggregation in this large Kn regime.

The purpose of this paper is to describe work in which the absolute value of the aggregation rate for an aerosol near the free molecular regime was measured with light scattering and full account of the fractal nature of the particles was made in the light scattering analysis. Moreover, once analyzed, the results are compared to aggregation theory which also attempts to account for the fractal aggregate nature. The measurements are obtained from a soot aerosol in a flame, hence the high temperature puts the kinetics at the boundary between the free molecular and Epstein regimes. The comparison between theory and experiment is good although considerable uncertainties exist both in the data, due largely to the uncertainty in the soot particle refractive index, and in the theory due to uncertainties in the effective radius for cluster mobility and collisional and particle absorption cross sections. Despite these uncertainities, this work experimentally establishes the validity of the aggregation kinetics for fractal aggregates in rarefied gases.

Given the broad range of subjects necessary to complete this study and the density of the material in each subject, a heuristic overview is worthwhile. We start by discussing the Smoluchowski equation which describes the temporal evolution of the cluster size distribution. We use self-preserving solutions to this equation to study the evolution of the moments of the distribution. It is the moments that any measurement measures hence they are key variables. We then show how the aggregation kernel can be determined from the moment evolution.

Next we discuss the theoretical form of the aggregation kernel which will be compared to the experiment. As mentioned above the kernel is rich in its functionality which is dependent upon how the clusters move. This in turn is dependent upon the cluster radius which, given the irregular cluster outline, is ambiguous. We spend some effort discussing this ambiguity.

Next we describe our light scattering technique which was developed in our laboratory. By combining structure factor measurements (scattered intensity versus angle, analogous to Bragg scattering) and absolute scattering and extinction measurements, complete morphological and number density information can be obtained for the soot clusters. All the data are obtained via light scattering, thus there is no perturbation to the soot aerosol.

Finally, analysis and measurement are combined to yield the experimental aggregation kernel as a function of cluster size for comparison to the theory.

THEORETICAL BACKGROUND

Irreversible aggregation dynamics is described by the Smoluchowski equation (Drake, 1972)

$$\frac{\partial n(v,t)}{\partial t} = \frac{1}{2}\int_0^v K(v-u,u)\, n(v-u,t)\, n(u,t)\, \mathrm{d}u - n(v,t)\int_0^\infty K(v,u)\, n(u,t)\, \mathrm{d}u. \tag{2}$$

In equation (2) $n(v, t)$ is the number density of aggregates of "size" v at time t, and $K(v, u)$ is the aggregation (collision) kernel which describes the rate at which aggregates of size v and u combine to form new aggregates of size $v + u$. Size may be measured in terms of cluster mass, volume, or number of monomers per cluster. An important property of the kernel is that for most physical situations the kernel is a homogeneous function of its variables, that is

$$K(av, au) = a^\lambda K(v, u). \tag{3}$$

The homogeneity constant of the kernel is λ, and this variable is important in the kinetics of growth and the resulting size distribution.

At sufficiently long times, the homogeneity condition (3) allows so-called scaling (van Dongen and Ernst, 1985) or self-preserving (Friedlander and Wang, 1966; Lai *et al.*, 1972; Friedlander, 1977) solutions to the Smoluchowski equation (2) of the form

$$n(v, t) = M_1 s_p^{-2} \phi(x). \tag{4}$$

In equation (4) x is the normalized or reduced size

$$x = v/s_p \tag{5}$$

and s_p is one of a class of mean sizes indexed by p and defined by

$$s_p(t) = M_p/M_{p-1} \tag{6}$$

where the unnormalized ith moment of the size distribution is given by

$$M_i(t) = \int_0^\infty v^i\, n(v, t)\, \mathrm{d}v. \tag{7}$$

Also in equation (4) is the reduced size distribution function $\phi(x)$ given by

$$\phi(x) = A\, x^\lambda\, \mathrm{e}^{-\alpha x} \tag{8}$$

for large x. The shape of $\phi(x)$ is not a function of time, hence the distribution is "self-preserving". The time dependence resides solely in the mean size $s_p(t)$. The large x regime is all we need to be concerned with in our study because light is scattered predominantly from the large size part of the cluster distribution. Moreover, the nature of the aggregation kernel in all three kinetic regimes is such that "bell shaped" distributions result characterized by exponentially decreasing cluster populations with decreasing size (van Dongen and Ernst, 1985). The parameters A and α in equation (8) are determined by normalization of the size distribution and the definition of the mean size s_p through p. Some detail is given in Appendix A. Our work involves light scattering, which essentially dictates that we use $p = 2$. This results because in the Rayleigh scattering regime, accessible for any particle or cluster at small enough scattering angle (see below), the scattered intensity goes as v^2 (Sorensen, 1997). Hence the mean size is $s_2 = M_2/M_1$, the so-called z-average size. Then, as shown in Appendix A,

$$\alpha = 2 - \lambda, \tag{9}$$

$$A = \alpha^\alpha/\Gamma(\alpha). \tag{10}$$

where Γ is the Gamma function.

A colligative measurement such as light scattering measures a moment of the distribution, M_i, not the distribution itself, $n(v)$. Thus we must understand the time evolution of the moments. This can be done by multiplying the Smoluchowski equation (2) by v^i and integrating over v to obtain

$$\dot{M}_i(t) = \frac{1}{2}\int_0^\infty \int_0^\infty [(v+u)^i - v^i - u^i]\, K(v,u)\, n(v,t)\, n(u,t)\, \mathrm{d}v\, \mathrm{d}u \tag{11}$$

where the overdot means time derivative. From equation (11) $\dot{M}_1(t) = 0$, as expected physically since M_1 represents the total number of primary particles in the system, which does not change due to aggregation (i.e. mass conservation). Again, our light scattering experiment will be concerned with the second moment, so we consider it here. (Appendix B also discusses the behavior of the zeroth moment which represents the number of aggregates and is an important case as well.) Also in Appendix B we show how equation (11) is modified under the assumption of kernel homogeneity and size distribution scaling. The results for $i = 2$ are

$$\dot{M}_2(t) = s_2^\lambda I_2 \tag{12a}$$

where

$$I_2 = \int_0^\infty \int_0^\infty xy\, K(x,y)\, n(x)\, n(y)\, \mathrm{d}x\, \mathrm{d}y. \tag{12b}$$

Since our goal is to determine the aggregation kernel K from a measurement of $\dot{M}_2(t)$, we follow Appendix B and rewrite equation (12a) as

$$K(s_2, s_2) = M_1^{-2}\, \dot{M}_2(t)/P_2 \tag{13a}$$

where

$$P_2 = I_2/K(1,1). \tag{13b}$$

In fact, with light scattering, we do not measure M_2 but rather a quantity we shall call the cluster number density $n_2 = M_1^2/M_2$. From equation (13a) one finds

$$K(s_2, s_2) = P_2^{-1} \frac{\mathrm{d}}{\mathrm{d}t}\left(\frac{1}{n_2}\right). \tag{13c}$$

Equations (13) show that by measuring the cluster number density optically as a function of time the aggregation kernel for a mean size s_2 can be determined. This analysis can be accomplished graphically by plotting inverse n_2 versus time, the slope yielding $P_2 K(s_2, s_2)$. This requires calculation of the polydispersity factor P_2 which in turn requires knowledge of the functional form of the kernel $K(x, y)$. Thus the situation is somewhat circular but not completely so because the all important magnitude of the kernel is not involved in P_2. [It is in I_2 and $K(1, 1)$ but these cancel in equation (13b).] In Appendix B we describe how we calculate P_2 and give numerical values. Also in Appendix B we show how this analysis is related to simpler and more often used but not as accurate analyses that assume a monodisperse distribution.

THE AGGREGATION KERNEL

The aggregation kernel describes the rate at which two aggregates combine to form a larger aggregate. Its properties are determined by the properties of the embedding fluid, the sizes and morphology of the clusters, and the manner in which the clusters move in the fluid. In what follows we describe the aggregation kernel first qualitatively, to gain physical insight, and then quantitatively, necessary for our data analysis. The qualitative nature of the aggregation kernel is illustrated in Fig. 1. The cluster motion depends on cluster morphology and the ratio of the mean free path (mfp) of the fluid molecules to the cluster radius, the Knudsen number $\mathrm{Kn} = \mathrm{mfp}/R$, and, in more rarefied fluids, the ratio of the

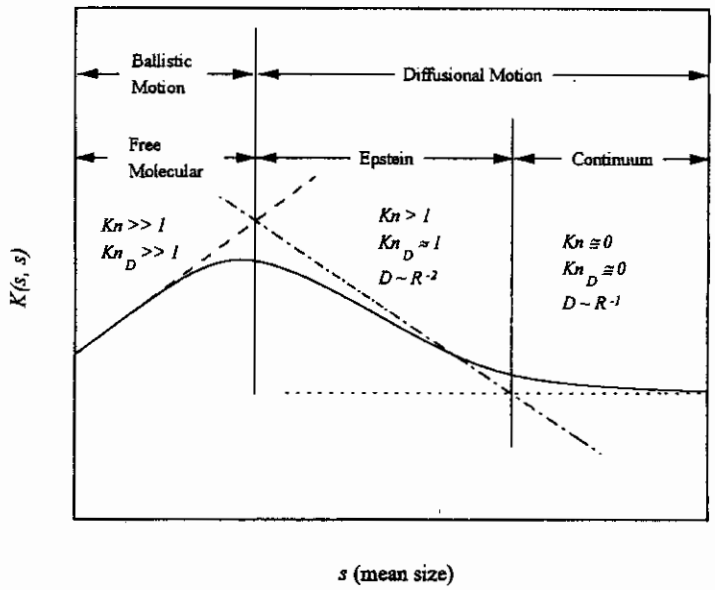

Fig. 1. Schematic diagram of the aggregation kernel for same size clusters as a function of size. Solid line is the complete kernel, long dashed line is the free molecular limit, dot dashed line is the Epstein limit, and short dashed line is the continuum limit.

cluster mean free path, or persistence length, to the cluster radius, the so-called diffusion Knudsen number $\mathrm{Kn_D}$. These two length scale comparisons divide the aggregation kernel functional dependence on size into three major regimes: diffusional motion with a Stokes–Einstein diffusion coefficient, diffusional motion with an Epstein diffusion coefficient, and ballistic motion. In dense fluids and/or for large clusters so that $\mathrm{Kn_D} \simeq 0$, the first two regimes are governed by diffusion of the clusters. Solution of the diffusion equation for one cluster of radius R diffusing relative to another yields an aggregation kernel with a general behavior of $K \sim DR$, where D is the cluster diffusion coefficient. These two diffusional regimes are differentiated by the Knudsen number Kn since for $\mathrm{Kn} \simeq 0$, $D \sim R^{-1}$ via the Stokes–Einstein equation, whereas for $\mathrm{Kn} \gg 1$, $D \sim R^{-2}$ via the Epstein equation. The crossover between these regimes, the transition regime, is described by the Cunningham correction to the Stokes–Einstein equation. In highly rarefied fluids (gases) such that $\mathrm{Kn_D} \gg 1$ the clusters travel in straight lines between collisions (ballistic aggregation) hence diffusional motion is lost. In this so-called free molecular regime the general behavior of the kernel is given by $K \sim cA$ where c is the average relative speed of the clusters, determined by equipartition, and A is the cluster collisional cross section. These three regimes impart aggregation phenomena with a wealth of interesting detail.

We consider a cluster of monomer particles, thus the number of monomers per cluster, N, is a proper measure of size. For aggregates that coalesce to dense spherical particles, e.g. liquid droplets, the relation $N \sim R^3$ can be used to find the kernel's functional dependency on size N for the three regimes. These dependencies are: $K_c \sim N^0$, $K_E \sim N^{-1/3}$ and $K_{fm} \sim N^{1/6}$ for the continuum, Epstein (also called the transition regime), and free molecular regimes, respectively. For fractal aggregates, however, the problem is not as straightforward because, although the simple relation $N \sim R^{D_f}$ holds, both the diffusion coefficients and the nature of the collisional radius or cross sectional area must be generalized from their well known spherical particle values to forms that apply to fractal aggregates. These generalizations have been studied previously and applied to computer simulations of aggregation (Mulholland *et al.*, 1988; Rogak and Flagan, 1992; Wu and Friedlander, 1993). We describe the current state of knowledge and our opinion of these issues below.

In the continuum regime diffusion is governed by the Stokes–Einstein equation

$$D_{SE} = \frac{k_B T}{6\pi\eta R} \tag{14}$$

where k_B is Boltzmann's constant, T the temperature, η the fluid shear viscosity and R the spherical particle radius. For aggregates this equation can be simply generalized by replacing R with R_m, the mobility radius of the aggregate. The most direct experimental test of this was given by Wiltzius (1987) who studied colloidal gold fractal aggregates in water over a size range of 60–800 nm. These aggregates had a fractal dimension of $D_f = 2.1$. He found the Stokes–Einstein equation to hold. A reanalysis of his data to account for the effects of cluster polydispersity on this analysis (Chen *et al.*, 1987; Pusey *et al.*, 1987) yielded a mobility radius of

$$R_m = \varepsilon R_g \tag{15}$$

with $\varepsilon = 0.97$. In their review of the Wiltzius result, other less direct data, and computer simulations (Chen, *et al.*, 1984, 1988; Meakin *et al.*, 1985), Rogak and Flagan (1992) concluded that $\varepsilon = 0.77$ for $D_f = 1.8$.

When $\mathrm{Kn} > 0$, the Cunningham correction formula can be used to transform the Stokes–Einstein equation into the Epstein equation, equation (18), as Kn increases (Seinfeld, 1986). Thus

$$D = D_{SE} C(\mathrm{Kn}), \tag{16}$$

$$C(\mathrm{Kn}) = 1 + 1.257\,\mathrm{Kn} + 0.4\exp(-1.1/\mathrm{Kn}), \tag{17}$$

$$D_E = \frac{3}{8\rho R^2 \delta}\left(\frac{k_B T m}{2\pi}\right)^{1/2}. \tag{18}$$

In equation (18) ρ is the fluid mass density, m the fluid molecular mass, and $\delta = (1 + \pi\alpha/8)$ where $0 \leqslant \alpha \leqslant 1$ is the accommodation coefficient. We shall use $\alpha = 0.91$ since then equations (16) and (17) yield equation (18) exactly in the $\mathrm{Kn} \to \infty$ limit. As with the Stokes–Einstein equation, the Epstein equation is for spherical particles of radius R. For clusters it is reasonable to once again replace R with a mobility radius R_m and ask in what manner R_m depends on the cluster morphology. In previous work from this laboratory (Cai and Sorensen, 1994) soot fractal aggregates with $D_f = 1.8$ were studied with both static light scattering, which measures R_g, a, and N, and dynamic light scattering, which measures D, to determined R_m for the Epstein equation. We found

$$R_m = \varepsilon a N^x \tag{19}$$

with $\varepsilon = 0.99 \pm 0.08$ and $x = 0.43 \pm 0.4$. This result was interpreted as physically due to the effective cluster cross section seen by a gas molecule impinging on the cluster, i.e., a "projected" cross section. It is in good agreement with projected cross sections of Meakin *et al.*, (1989) who examined computer simulated clusters and is also in good accord with the estimate made by Rogak and Flagan (1992) for R_m (their Fig. 3). Note, however, the dependency of equation (19) on N is different than the radius of gyration which is $R_g = 1.16\, aN^{0.55}$ for $D_f = 1.8$. Cai and Sorensen (1994) found that the ratio R_m/R_g varied from 1.1 to 0.7 as the clusters increased from 3 to 30 monomers per cluster. All these results imply that for small clusters $R_m = R_g$ is a reasonable approximation, but a more exact treatment would require the use of equation (19) in equation (18).

Next there is the problem of what to use for the effective absorbing sphere radius R_{abs}, the boundary to which the clusters diffuse during aggregation. Again, the answer is obvious for spherical, compact clusters, since R_{abs} is that cluster's radius. For fractal clusters others have assumed this absorption radius to be R_g, i.e., $R_{abs} = R_g$. This, however, is certainly wrong for spheres since then $R_g = \sqrt{3/5}\, R$. Rogak and Flagan (1992) argued that the absorption radius is bounded by the mobility radius at the lower limit and the outer, or perimeter, radius at the upper limit. We regard this latter radius as poorly defined due to the

nonspherical symmetry of the cluster and its indefinite outline. They showed that for $D = 1.8$ comparison to simulated clusters of Meakin *et al.* (1989) was best at the lower limit, mobility radius R_m, although at most 30% larger. Recall $R_m \sim 0.77$ to $0.97\,R_g$ in the continuum regime and the Cai and Sorensen (1994) experiment for which $R_m \sim 0.7$ to 1.1 R_g for clusters of size $30 > N > 3$ in the Epstein regime. Hence a reasonable and simple conclusion is $R_{abs} = R_g$ for fractal aggregates.

Transition into the free molecular regime means the cluster move ballistically rather than diffusionally and the generic behavior of the kernel is $K \sim cA$. Equipartition will still hold for fractal clusters as it does for dense spheres so the kinetic theory result for the speed term should still hold. Thus

$$K(v, u) = \left(\frac{8\pi k_B T}{m_v} + \frac{8\pi k_B T}{m_u}\right)^{1/2} A_{vu}. \tag{20}$$

The mass is given by $m = N\rho_s 4\pi a^3/3$ where ρ_s is the monomer mass density.

As above, the problem of how to generalize the spherical particle result to fractal aggregates leads to uncertainty for the form of the collision cross section A. The simplest generalization, used previously by others (Mulholland *et al.*, 1988), is that

$$A_{vu} = \pi (R_{g,v} + R_{g,u})^2, \tag{21}$$

i.e. the spherical dense cluster radius is replaced by the fractal cluster radius of gyration, R_g. We have already noted above that this approximation has the wrong spherical particle limit since $R_g = \sqrt{3/5}\,R$, however, a lot changes as D_f evolves from 3 to 1.8. Given our ignorance and the simplicity of equation (21) we have no recourse other than to use equation (21) for fractal aggregates.

It has been argued (Mulholland *et al.*, 1988) that equation (21) is satisfactory when $D_f \geqslant 2$ because then the clusters are projectionally dense, i.e. a small particle on a straight line path toward the clusters could not pass through it. If $D_f < 2$, it is proposed that

$$A_{vu} = \pi(R_{g,v} + R_{g,u})^{D_f}. \tag{22}$$

This form accounts for the nondense nature of the two-dimensional projection of a given cluster that another cluster would see as it approaches during an impending collision. It also saves the kernel from a nonphysical dependency on size when one cluster is vastly greater than the other. There are disadvantages to using equation (22) as well. It causes a discontinuity in the dependency of the polydispersity exponent λ in the scaling equation (equation (8)) for the size distribution at $D_f = 2$. Furthermore, the arguments regarding projection density are based on asymptotically large clusters. The simulations of Meakin *et al.* (1989) have shown that finite sized clusters ($N \lesssim 2500$) with $D_f \simeq 1.8$ are projectionally dense (i.e. monomer–monomer screening occurs). The Cai and Sorensen (1994) work on diffusion of soot clusters showed that whereas $D_f = 1.8$ the projectional area which determined the mobility radius was dense and had an effective fractal dimension of $(0.43)^{-1} = 2.3$. Thus we believe equation (21) is more correct than equation (22) and shall use it in our analysis.

In summary, consideration of cluster mobility and size involved in all three regimes of aggregation shows that the radius of gyration is to a factor of unity an accurate measure for both mobility and size, and, although imperfect, it is the best measure available so far. Thus we shall use R_g in place of the spherical particle radius R in the equations for the aggregation kernel.

We are now ready to write the complete aggregation kernel and its limits. The complete form is (Seinfeld, 1986)

$$K(v, u) = 4\pi D_{vu} R_{vu} \beta. \tag{23}$$

In (23) $D_{vu} = D_v + D_u$ where D_v is the diffusion coefficient for clusters of size v, and $R_{vu} = R_v + R_u$ where R_v is the absorbing radius for clusters of size v. The diffusion coefficient is given most generally by equation (16) with limits at Kn = 0 of Stokes–Einstein,

equation (14), and at $\mathrm{Kn} \gg 1$ of Epstein, equation (18). These are referred to as the continuum and transition regimes, respectively. Recall from the argument immediately above that all radii will be the cluster radius of gyration R_g.

Also in equation (23) is the factor β which transforms the diffusive aggregation to ballistic aggregation. Two forms, one due to Fuchs (1964) the other Dahneke (1983), are available for β and they agree with each other to within 4%. We choose the Dahneke form due to its simplicity:

$$\beta = \frac{1 + \mathrm{Kn_D}}{1 + 2\mathrm{Kn_D}(1 + \mathrm{Kn_D})}. \tag{24}$$

The diffusive Knudsen number is

$$\mathrm{Kn_D} = \frac{2D_{vu}}{c_{vu} R_{vu}} \tag{25}$$

where c_{vu} is the mean relative speed between clusters of size v and u given by

$$c_{vu} = \left(\frac{8k_B T}{\pi}\right)^{1/2} (m_v^{-1} + m_u^{-1})^{1/2}. \tag{26}$$

For small $\mathrm{Kn_D}$, $\beta = 1$ and the aggregation is diffusive $K \sim DR$; however, for large $\mathrm{Kn_D}$, $\beta = (2\mathrm{Kn_D})^{-1} = C_{vu}R_{vu}/4D_{vu}$ and this limit replaces diffusive motion with straight line, ballistic motion so that $K \sim cR^2$. Table 1 summarizes the aggregation kernel and its three regimes.

Table 1. The aggregation kernel

General form

$$K(v, u) = 4\pi D_{vu} R_{vu} \beta \tag{23}$$

$$D_{vu} = D_v + D_u$$

$$R_{vu} = R_v + R_u$$

$$D_v = \frac{k_B T}{6\pi\eta R_v} C(\mathrm{Kn}) \tag{16}$$

$$C(\mathrm{Kn}) = 1 + 1.257\,\mathrm{Kn} + 0.4\exp(-1.1/\mathrm{Kn}) \tag{17}$$

$$\mathrm{Kn} = \mathrm{mfp}/R$$

$$\beta = \frac{1 + \mathrm{Kn_D}}{1 + 2\,\mathrm{Kn_D}(1 + \mathrm{Kn_D})} \tag{24}$$

$$\mathrm{Kn_D} = 2D_{vu}/c_{vu}R_{vu} \tag{25}$$

$$c_{vu} = (8k_B T/\pi)^{1/2} (m_v^{-1} + m_u^{-1})^{1/2} \tag{26}$$

Limits

1. Continuum, $\mathrm{Kn} = 0$, $\mathrm{Kn_D} = 0$

$$K(v, u) = (2k_B T/3\eta)(R_v^{-1} + R_u^{-1})(R_v + R_u).$$

If fractal clusters $K(v, u) = (2k_B T/3)(v^{-1/D_f} + u^{-1/D_f})(v^{1/D_f} + u^{1/D_f})$

2. Transition, $\mathrm{Kn} \gg 1$, $\mathrm{Kn_D} = 0$

$$K(v, u) = \frac{\pi}{2\rho\delta}\left(\frac{k_B T m}{2\pi}\right)^{1/2} (R_v^{-2} + R_u^{-2})(R_v + R_u).$$

If fractal clusters

$$K(v, u) = \frac{\pi}{2\rho\delta}\left(\frac{k_B T m}{2\pi}\right)^{1/2} a^{-1} k_0^{-1/D_f} (v^{-2/D_f} + u^{-2/D_f})(v^{-1/D_f} + u^{1/D_f})$$

3. Free molecular, $\mathrm{Kn} \gg 1$, $\mathrm{Kn_D} \gg 1$

$$K(v, u) = (8\pi k_B T)^{1/2} (m_v^{-1} + m_u^{-1})^{1/2} (R_v + R_u)^2$$

If fractal clusters

$$= (6k_B T/\rho)^{1/2} a^{1/2} k_0^{-2/D_f} (v^{-1} + u^{-1})^{1/2} (v^{1/D_f} + u^{1/D_f})^2.$$

LIGHT SCATTERING

Our light scattering measurements and analysis take full account of the fractal nature of the soot clusters. An optical structure factor technique (Gangopadhyay *et al.*, 1991), which yields cluster radius of gyration and fractal dimension, and the classic scattering/extinction method (D'Alessio *et al.*, 1975; D'Alessio, 1981), which yields a volume equivalent sphere and cluster number density, when combined also yields the average number of monomers per cluster and the monomer size (Sorensen *et al.*, 1992a). This method has been firmly established by comparison to electron microscope analysis of soot thermophoretically sampled from a flame (Cai *et al.*, 1993).

In the limit of small monomers compared to the wavelength of light, e.g. monomers that are Rayleigh scatterers, the relation between monomer and cluster scattering and absorption cross sections is quite simple (Berry and Percival, 1986; Sorensen, 1997). The differential scattering cross section, $\sigma_s^c(\theta)$, of the cluster is

$$\sigma_{sca}^{c}(\theta) = N^2 \sigma_{sca}^{mon} S(qR_g) \tag{27}$$

and the cluster absorption cross section is

$$\sigma_{abs}^{c} = N \sigma_{abs}^{mon}. \tag{28}$$

In the above N is the number of monomers per cluster, the superscripts c and mon refer to cluster and monomer, respectively, θ is the scattering angle, $q = 4\pi\lambda^{-1} \sin\theta/2$ is the scattering wave vector, and $S(qR_g)$ is the static structure factor which obeys

$$S(qR_g) = 1 \qquad \text{for } qR_g \ll 1, \tag{29a}$$

$$S(qR_g) \simeq 1 - q^2R_g^2/3 \quad \text{for } qR_g \lesssim 1, \tag{29b}$$

$$S(qR_g) \sim q^{-D_f} \qquad \text{for } qR_g > 1. \tag{29c}$$

The exact form of the structure factor is dependent on the manner in which the density correlation function of the cluster cuts off at its perimeter. We have found (Sorensen *et al.*, 1992b; Cai *et al.*, 1995) that this is well approximated by a Gaussian which leads to a structure factor given by

$$S(x) = e^{-x^2/D_f}\, {}_1F_1(3/2 - D_f/2, 3/2; x^2/D_f) \tag{30}$$

where ${}_1F_1$ is the confluent hypergeometric series. For the monomeric Rayleigh scatterers the cross sections are (Kerker, 1969)

$$\sigma_{sca}^{mon} = k^4 a^6 F(m), \tag{31}$$

$$\sigma_{abs}^{mon} = 4\pi k a^3 E(m) \tag{32}$$

where $F(m) = |(m^2 - 1)/(m^2 + 2)|$ and $E(m) = -\text{Imag}\{(m^2 - 1)/(m^2 + 2)\}$ with m the complex refractive index of the particles. Also $k = 2\pi/\lambda$ and a is the monomer radius. Proper use of equations (27)–(32) allows for a complete characterization of the soot cluster morphology as described below.

The cluster radius of gyration can be obtained from the structure factor which in the Guinier regime, where $qR_g^2 \lesssim 1$, obeys equation (29b). A graph of I^{-1} vs q^2 for the data in this regime yields linearity with a slope of $R_g^2/3$ (Gangopadhyay *et al.*, 1991). The soot aerosol is polydisperse hence any measurement involves a measurement of size distribution moments. The radius of gyration is measured in the small angle regime where the cluster scattering goes as N^2, i.e. the Rayleigh regime of the cluster. This acts as a weighting factor in calculating the average of R_g^2 which by equation (1) equals $a^2 k_0^{-2/D_f} N^{2/D_f}$. Thus the R_g measurement involves the $2 + 2/D_f$ moment normalized by the second moment as

$$R_{g,meas}^2 = a^2 k_0^{2/D_f} \frac{M_{2+2/D_f}}{M_2}. \tag{33}$$

Scattering/extinction measurements are best performed in the small angle regime such that $qR_g \ll 1$ so that $S(qR_g) = 1$. Then the optical power P_s scattered from a beam of incident intensity I_0 measured by the detector is obtained from equations (27), (29) and (31) to be

$$P_s = I_0 c_0 n N^2 k^4 a^6 F(m) \quad \text{(monodisperse)} \tag{34a}$$

$$= I_0 c_0 M_2 k^4 a^6 F(m) \quad \text{(polydisperse)} \tag{34b}$$

where c_0 is a calibration constant involving the solid angle of detection and the efficiency of the detector. Its value is determined by scattering from gases of known Rayleigh Ratio. Also in equation (34) is n the cluster number density, a moment ratio yet to be defined.

The extinction measurement is performed by comparing the incident and transmitted light after it passes through a length ℓ of the flame

$$I_T = I_0 e^{-\tau \ell}. \tag{35}$$

The turbidity τ is related to both the absorption and total scattering cross section and the soot cluster number density n by

$$\tau = n(\sigma^c_{abs} + \sigma^c_{sca}). \tag{36}$$

Usually the approximation $\sigma_{abs} \gg \sigma_{sca}$ is made, but we will forego this since we have found this makes as much as a 30% error for our largest clusters. To calculate the total scattering cross section σ_{sca} we use an integration over all solid angle

$$\sigma^c_{sca} = \int \sigma^c_{sca}(\theta)\, d\Omega. \tag{37}$$

To perform this integration analytically we use the so-called Fisher–Burford form for the structure factor, $S(x) = (1 + 2x^2/3D_f)^{-D_f/2}$. This makes the integration easy to perform analytically. This form results from a fractal cluster with a density correlation function with an exponential cutoff. We have shown such a function to be inaccurate for angular scattering studies, but this inaccuracy does not significantly propagate into the total scattering calculation. For incident light polarized perpendicular to the scattering plane which embeds θ equation (37) yields

$$\sigma^c_{sca} = \frac{8\pi}{3}\left(1 + \frac{4k^2R_g^2}{3D_f}\right)^{-D_f/2} \tag{38a}$$

$$= 4\pi g. \tag{38b}$$

A combination of the scattering and extinction measurements can yield the cluster number density and a volume equivalent sphere radius. The number density so measured n is in fact equal to a ratio of first and second moments of the distribution because scattering goes as N^2 and absorption as N (equations (27) and (28), respectively). By the logic in Appendix B, equation (B7), we shall hence forth call this number density $n_2 = M_1/s_2$. From equations (34b), (36) and (38) one finds

$$n_2 = \frac{M_1^2}{M_2} = \left(\frac{k}{4\pi}\right)^2 \frac{F}{E^2} \frac{(\tau - 4\pi g P_s/I_0 c_0)^2}{P_s/I_0 c_0} \tag{39}$$

and

$$R^3_{SE} = a^3 \frac{M_2}{M_1} = \frac{4\pi}{k^3} \frac{E}{F} \frac{P_s/I_0 c_0}{\tau - 4\pi g P_s/I_0 c_0}. \tag{40}$$

We call the volume equivalent sphere radius R_{SE}, the scattering/extinction radius. Measurement of P_s, I_0, c_0 and τ with knowledge of the soot refractive index to calculate E and F allows n and R_{SE} to be determined.

R_{SE} contains the important mean size $s_2 = M_2/M_1$. If the monomer radius a is known, the mean size can be extracted directly from R_{SE}. The monomer radius can be determined by either collecting the soot from the flame and inspecting it with electron microscopy or via *in situ* optical measurements. Although there is always concern about perturbing the flame, we have shown these two measurements to be consistent (Cai *et al.*, 1993). The optical technique that we have used to determine a, hence mean size s_2, also yields the fractal dimension. This is the method we use here.

Our analysis (Sorensen *et al.*, 1992a) is to view equations (1) and (40) as two equations with two unknowns, the monomer radius a and the mean size $N = s_2 = M_2/M_1$. R_{SE} and R_g are measured with light scattering. However, equation (33) shows that the measured $R_{g,meas}$ is not equal to the R_g defined in equation (1) because light scattering weights the cluster size distribution in a particular manner. Thus to use the two equations two unknowns concept the moments involved in $R_{g,meas}$, $M_{2+2/D_f}/M_2$, must be related to the mean size.

To achieve this conversion to mean size the general expression for the ith moment given in Appendix A is used. To calculate the moments we assume the well established scaling distribution. In the past (Sorensen *et al.*, 1992a) we have stressed that the usually used log normal distribution would fail here. The reason for this is that the log normal distribution is an approximation to the exact scaling distributions, and it begins to give grossly erroneous results for moments higher than the second. R_g involves $M_{2+2/D_f} \sim M_3$ hence scaling must be used. Needed next is the kernel homogeneity which determines the distribution width, λ in equation (8). Here a self-consistent argument is made. Our final results are in a regime for which the kernel is not a strong function of size hence $\lambda \simeq 0$, so this value will be used to calculate the moments. This calculation yields

$$\frac{M_{2+2D_f}}{M_2} = \frac{\Gamma(3 + 2/D_f)}{2^{1+2/D_f}} s_2^{2/D_f}. \tag{41}$$

Now equation (41) substituted into equations (33) and (40) represent two equations and two unknowns with solutions

$$s_2 = k_0^{-3/(3-D_f)} \left[\frac{\Gamma(3 + 2/D_f)}{2^{1+2/D_f}}\right]^{3D_f/2(3-D_f)} \left(\frac{R_g}{R_{SE}}\right)^{3D_f/(3-D_f)}, \tag{42}$$

$$a = k_0^{1/(3-D_f)} \left[\frac{2^{1+2/D_f}}{\Gamma(3 + 2/D_f)}\right]^{D_f/2(3-D_f)} \left(\frac{R_{SE}^3}{R_g^{D_f}}\right)^{1/(3-D_f)}. \tag{43}$$

Note that if a is constant, equation (43) implies that $R_{SE}^3 \propto R_{g,meas}^{D_f}$, and this can be used to determine D_f. Below (Fig. 6) we shall see that the experimentally determined a is constant over a region large enough to allow for an accurate measurement of D_f.

EXPERIMENTAL METHODS

The flame and light scattering techniques were similar to those used previously in our laboratory (Sorensen *et al.*, 1992a, b; Cai *et al.* 1993). The soot aerosol was created by a premixed ethylene and oxygen flame. This flame was supported on a McKenna Products burner with a 6 cm diameter porous frit. This frit was surrounded by an annular sheath 0.5 cm wide through which nitrogen flowed. A 15 cm diameter steel stagnation plate was placed 3.0 cm above the burner surface to stabilize the flame. The C/O ratio for the mixture was 0.77, and the cold gas flow velocity was 4.7 cm s^{-1}. This arrangement yields a quasi-one-dimensional flame with the only major variable being the height above burner. Temperature measurements were made with an optical pyrometer calibrated at our laser wavelength of 488 nm. The emissivity of the flame was the absorptivity of the flame as measured by laser extinction.

Light scattering used an argon ion laser with $\lambda = 488$ nm as a light source. Scattered light was measured at a variety of angles between 10 and 110° to yield the static structure factor. A Guinier analysis yields cluster radius of gyration via equation (29b). Absolute scattering measurements were performed at angles such that $qR_g < 1$, typically $\theta = 20°$; so that the scattering was in the Rayleigh regime, equations (27) and (29a). Calibration was made by scattering from gaseous N_2, O_2, CH_4 and C_2H_4 whose Rayleigh Ratios are known. Laser extinction was measured by comparing incident and transmitted intensites for the flame. The optical path in the flame was measured as a function of height above burner.

Laser Doppler velocimetry (LDV) was used to determine the residence time of the soot clusters in the flame. LDV measures the soot cluster velocity as a function of height above burner. This measurement can be integrated over height to yield the time. In our LDV measurement the $\lambda = 488$ nm beam was split into two equal intensity parallel beams with a mirror and beam-splitter arrangement. These two beams passed through a lens which focussed and crossed the beams at a half angle of $\gamma = 3.7°$. This caused a sinusoidal fringe pattern in a Gaussian envelope (the laser was in the TEM00 mode). The scattered intensity from this fringe pattern in the flame was analyzed with an ALV 5000 correlator. The intensity autocorrelation function of the scattered light was fit to

$$C(t) \sim \cos(\omega t)\, e^{-dt^2} \tag{44}$$

where d is a fit parameter irrelevant to the analysis. The speed is given by

$$V = \frac{\omega\lambda}{4\pi \sin\gamma}. \tag{45}$$

Lastly the time at height h relative to zero time at an arbitrary h_0 is given by

$$t = \int_{h_0}^{h} \frac{dh}{V(h)}. \tag{46}$$

DATA ANALYSIS AND RESULTS

Figure 2 shows the measured radius of gyration, $R_{g,meas}$, determined from the Guinier regime of the optical structure factor equation (29b) as a function of the height above burner h. The flame front was determined to be at $h = 2.0 \pm 0.5$ mm by visual inspection which agrees with the height where R_g extrapolates to zero, which was 3.0 mm. One can see over an order of magnitude growth from essentially monomeric particles to large clusters.

Figure 2 also shows the scattering extinction radius R_{SE} determined using equation (40) as a function of h. Recall this is the volume equivalent radius. We include both "uncorrected," i.e. under the assumption that scattering does not contribute to extinction, equation (40) with $g = 0$, and "corrected," i.e. the correct fact that extinction is due to both scattering and absorption, equation (40) with g given by equation (38), results. One can see that significant error can result for large clusters if scattering is not included.

Figure 3 gives the cluster number density $n_2 = M_2^1/M_2$ determined using equation (39) as a function of h both uncorrected and corrected for scattering effects in extinction. Again, significant error would occur if scattering effects were ignored. For both R_{SE} and n_2 the soot refractive index was assumed to be the Dalzell and Sarofim (1969) value of $m = 1.57–0.56i$. Later in our analysis of the aggregation kernel a range of refractive indices will be considered.

Figure 4 plots R_{SE}^3 versus R_g which on a log-log plot should have a slope of D_f according to equation (43). As will be seen below, the monomer radius a is changing for the first three points. Ignoring these, the relation is quite linear and yields $D_f = 1.89 \pm 0.1$, in reasonable agreement with previous work and that expected, $D_f = 1.8$, for DLCA clusters.

Figures 5 and 6 show the number of monomers per aggregate $N = s_2 = M_2/M_1$ and monomer radius a versus h both uncorrected and corrected for scattering effects in extinction. These are obtained from the analysis that yields equations (42) and (43), which include the effects of scattering on extinction. These plots are for mean values accounting for

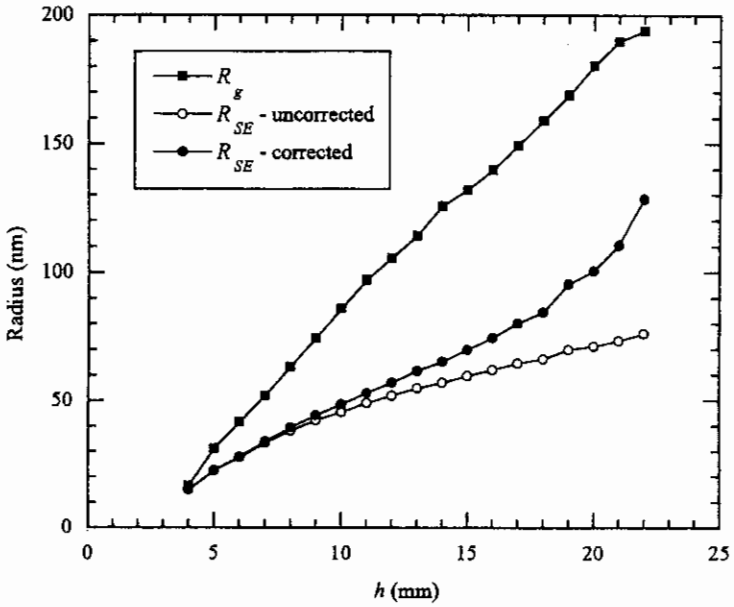

Fig. 2. Aggregate radius as a function of height above burner.

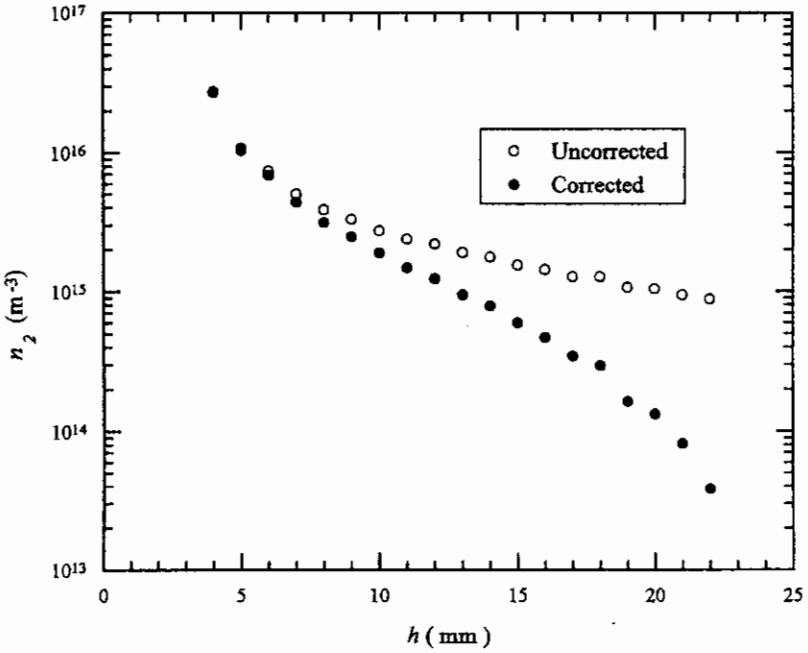

Fig. 3. Cluster number density as a function of height above burner.

the effects of polydispersity on the light scattering measurement. The size distribution assumed is scaling with $\lambda = 0$ in equation (8) which will be justified in our analysis of the aggregation kernel below. Figure 5 shows that the monomer grows at low heights, but this growth quickly levels off by $h \sim 7$ to 8 mm. The monomer size is in accord with that usually found (Dobbins and Megaridis, 1987; Koylu and Faeth, 1992; Cai *et al.*, 1993). The quickly saturated growth is reasonable given the chemical surface growth of soot early in the flame. The independence of monomer size above $h \sim 7$ to 8 mm implies surface growth of soot is no longer significant at larger h hence aggregation is the main growth mechanism. This is what we want for our study.

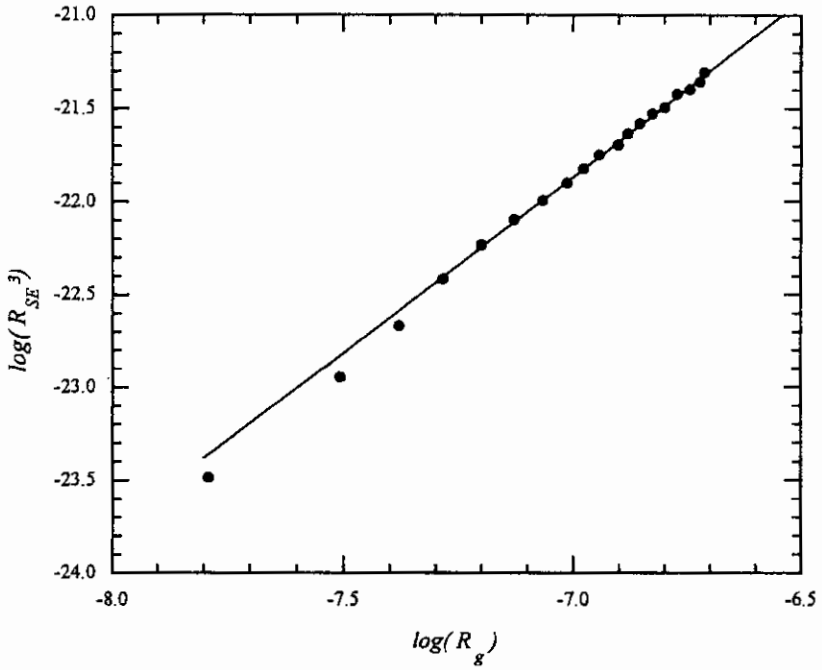

Fig. 4. Log–log plot of R_{SE} versus R_g. The line is a linear best fit to all but the first three points, and it has a slope of $D_f = 1.89 \pm 0.1$.

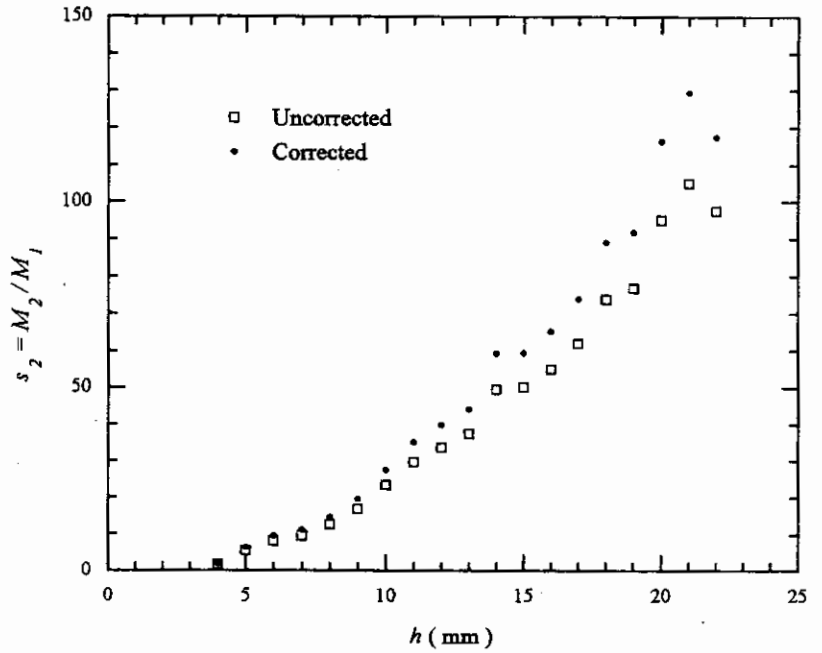

Fig. 5. The mean number of monomers per aggregate as a function of height above burner.

To obtain the aggregation kernel the inverse cluster number density n_2 is plotted versus time in Fig. 7. In accordance with equation (13c) the slope yields the product of the polydispersity factor and the kernel. The value of the polydispersity factor P_2 is taken from the Table B2 in Appendix B as an average of the Epstein and free molecular values, the range over which the data lie, and then the kernel is extracted from the slope. Also the mean

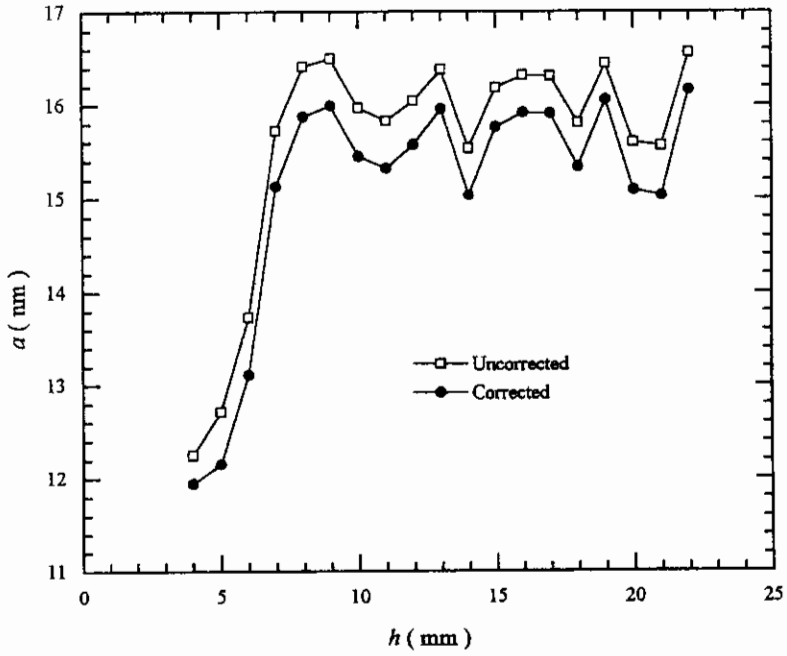

Fig. 6. The monomer radius as a function of height above burner.

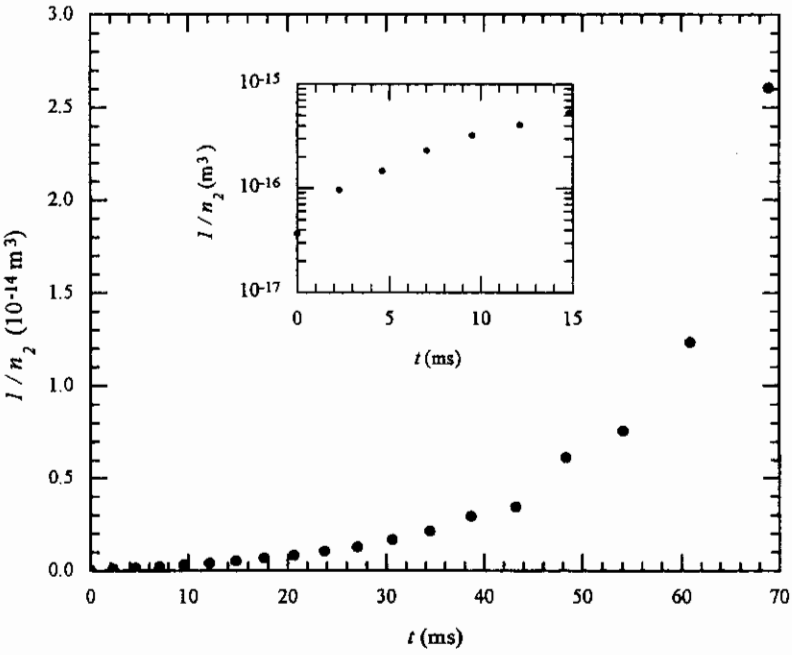

Fig. 7. Inverse cluster number density versus time.

size $s_2 = N$ of Fig. 6 is determined as a function of time by converting h to t. Then with both the kernel and the mean size as functions of time, they can be matched to yield the kernel as a function of mean size. This is our long sought result, and it is given in Fig. 8.

Our results are strongly influenced by the soot refractive index value used in the light scattering analysis. Values available in the literature vary widely, and this variation is independent of fuel type (Colbeck *et al.*, 1989; Vaglieco *et al.*, 1990; Koylu and Faeth, 1996). The range of possible refractive indices yields a range of experimental aggregation

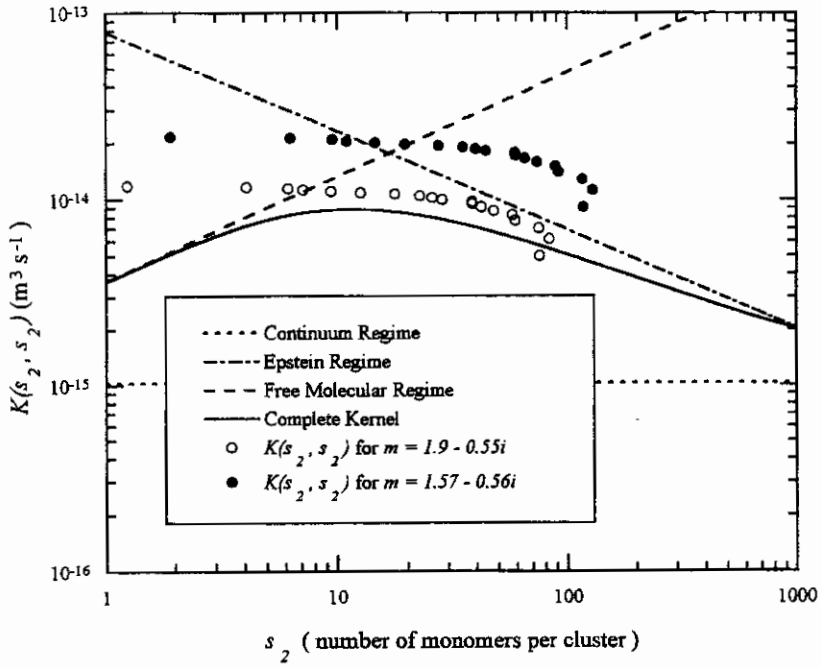

Fig. 8. The aggregation rate for equal sized clusters as a function of cluster size. Solid and open points are the experimental values derived from light scattering using the soot refractive index of either Dalzell and Sarofim (1969) or Vaglieco *et al.*. (1990), respectively. Theoretical lines are for the continuum, Epstein, and free molecular limits of the aggregation kernel, and the complete kernel (solid line). The Knudsen numbers for the experimental points range from 25 to 1.7

coefficients derived from our light scattering analysis. Over this broad range the Dalzell–Sarofim value of $m = 1.57–0.56i$ yields the largest aggregation coefficient values. On the other hand the refractive index of Vaglieco *et al.* (1990) $m = 1.9–0.55i$ yields the lowest aggregation coefficient values, a factor of two smaller than that derived from the Dalzell–Sarofim value. Thus this spread in uncertainty of the experimental $K(s_2, s_2)$ due to the uncertainty in soot refractive index is about a factor of two.

To compare the experimental results to theory we calculate the aggregation kernel according to the summary in Table 1. We calculate the kernel for equal sized clusters $K(s_2, s_2)$. The equations require R and this, as described above, is equal to R_g; hence via equation (1), $R_g = a\, k_0^{-1/D_f} s_2^{1/D_f}$. We use $k_0 = 1.3$ and the experimental values for a, s_2 and $D_f = 1.89$. Temperature is that measured by pyrometry shown in Fig. 9. The mean free path of the gas molecules was taken to be 410 nm and the viscosity of the gas 610 μP. These are values for air at 1700 K, roughly the average flame temperature. These values are not critical in our analysis since, as seen in Fig. 8, the kinetics are far from the continuum and Epstein regime where these values play a role. The cluster masses were determined from a carbon density of $\rho_s = 1.89\ \mathrm{g\,cm^{-3}}$, the monomer radius and the number of monomers per cluster s_2 as described below equation (20). All this detail feeds into equation (22) to allow $K(s_2, s_2)$ to be calculated and this calculation is shown in Fig. 8.

Comparison of theory and experiment shows the theory to be approximately a factor 1.15 to 2 too low. Changes in either theory or experiment due to uncertainties in the host of variables other than the refractive index lead to changes as large as 40%. Thus by far the major uncertainty is due to soot refractive index.

The data fall near the top of the "hump" in the curve of $K(s_2, s_2)$ versus s_2 as the free molecular regime transforms into the Epstein regime. Using the cluster radius of gyration the data lie in the Knudsen number range of 25 to 1.7. The data have very little size dependence consistent with theory in this crossover regime. Thus the $\lambda = 0$ approximation used above is justified. The data for small s_2 suffer somewhat from the fact that the fractal

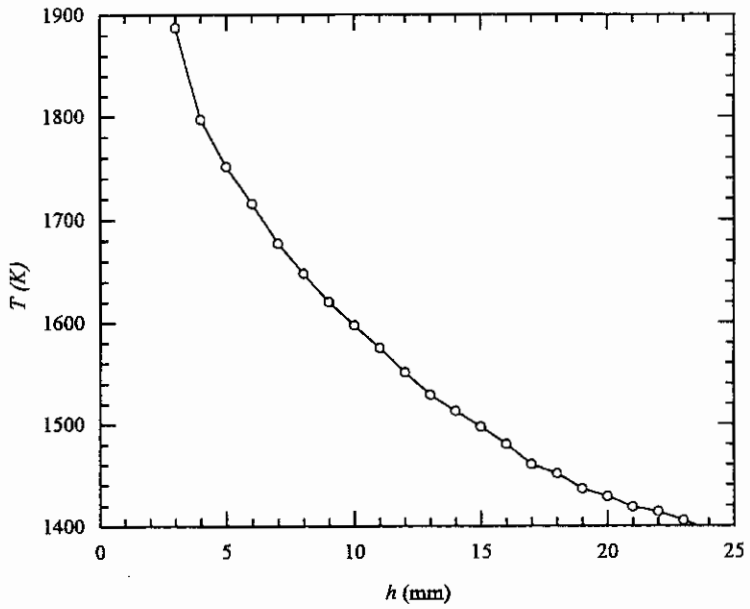

Fig. 9. Flame temperature as a function of height above burner.

description must breakdown as $s_2 \to 1$. At large size the data appear to be following the maximum in the theoretical curve. Certainly, the uncertainties induced by our much discussed concerns involving the proper R values for fractal aggregates above are not large enough to rectify the theory–experiment disparity nor are they large compared to the refractive index uncertainty. In light of the uncertainties and the broad range of the possible kernel values, the comparison in Fig. 8 establishes the validity of the theory for fractal aggregates in rarefied gases. The overall deviation could be ascribed to dispersion forces (Marlow, 1980a, b, 1981) that cause cluster–cluster attraction hence a larger aggregation kernel than that predicted by equation (23). The magnitude of a dispersion force effect is similar to the discrepancy in Fig. 8, but is difficult to quantify.

CONCLUSIONS

We find the aggregation kernel as described by the equations in Table 1 to yield a good description of the aggregation rate for a fractal aggregate soot aerosol in the crossover regime from the free molecular to Epstein regimes. The measurements were made *in situ* with static light scattering that took proper account of the fractal nature of the aggregate. The largest uncertainty was due to the poorly known value of the soot refractive index which caused a factor of two variation in the experimental aggregation kernel. The theoretical curve lies at the lower limit of this spread. The enhanced aggregation rate over theory could possibly be due to attractive dispersive forces between clusters.

Acknowledgements—This work was supported by NSF grant CTS9408153.

REFERENCES

Berry, M. V. and Percival, I. C. (1986) Optics of fractal clusters such as smoke. *Optica Acta* **33,** 577.

Bunz, H. (1990) Coagulation Workshop. Nuclear Research Center, Karlsruhe 16–18 March 1988. *J. Aerosol Sci.* **21,** 139.

Cai, J., Lu, N. and Sorensen, C. M. (1993) Comparison of size and morphology of soot aggregates as determined by light scattering and electron microscope analysis. *Langmuir* **9,** 2861.

Cai, J. and Sorensen, C. M. (1994) Diffusion of fractal aggregates in the free molecular regime. *Phys. Rev. E* **50,** 3397.

Cai, J., Lu, N. and Sorensen, C. M. (1995) Analysis of fractal cluster morphology parameters: structural coefficient and density autocorrelation function cutoff. *J. Colloid Inter. Sci.* **171,** 470.

Chen, Z.-Y., Deutch, J. M. and Meakin, P. (1984) Translational friction coefficient of diffusion limited aggregates. *J. Chem. Phys.* **80,** 2982.
Chen, Z.-Y., Meakin, P. and Deutch, J. M. (1987) Comment on "Hydrodynamic Behavior of Fractal Aggregates". *Phys. Rev. Lett.* **59,** 2121.
Chen, Z.-Y., Weakliem, P. C. and Meakin, P. (1988) Hydrodynamic radii of diffusion-limited aggregates and bond percolation clusters. *J. Chem. Phys.* **89,** 5887.
Colbeck, I., Hardman, E. J. and Harrison, R. M. (1989) Optical and dynamical properties of fractal clusters of carbonaceous smoke. *J. Aerosol Sci.* **20,** 765.
D'Alessio, A., DiLorenzo, A., Sarofim, A. F., Beretta, F., Masi, S. and Venitozzi, C. (1975) Soot formation in methane–oxygen flames. *Proc. 15th Int. Symp. on Combustion,* Combustion Institute, Pittsburg, PA, p. 1427.
D'Alessio, A. (1981) In *Laser Light Scattering and Fluorescence Diagnostics of Rich Flames Particulate Carbon,* (Edited by Siegla, D. C. and Smith, G. W.) p. 207. Plenum, New York.
Dahneke, B. (1983) Simple kinetic theory of brownian diffusion in vapors and aerosols. In *Theory of Dispersed Multiphase Flow,* (Edited by Meyer R. E.) p. 97. Academic Press, New York.
Dalzell, W. H. and Sarofim, A. F. (1969) Optical constants of soot and their application to heat-flux calculations. *J. Heat Transfer* **100,** 104.
Dobbins, R. A. and Megaridis, C. M. (1987) Morphology of flame-generated soot as determined by thermophoretic sampling. *Langmuir* **3,** 254.
Drake, R. L. (1972) A general mathematical survey of the coagulation equation. In *Topics in Current Aerosol Research,* Vol. 3, p. 208 (Edited by Hidy, G. M. and Brock, J. R.) Pergamon, New York.
Family, F. and Landau, D. P. (1984), eds., *Kinetics of Aggregation and Gelation.* North-Holland, Amsterdam.
Feldermann, C., Jander, H. and Wagner, H. G. (1994) Soot particle coagulation in premixed ethylene/air flames at 10 bar. *Z. Phys. Chemie* **186,** 127.
Forrest, S. R. and Witten, T. A. (1979) Long-range correlations in smoke-particle aggregates. *J. Phys. A* **12,** L109.
Friedlander, S. K. and Wang, C. W. (1966) The self-preserving particle size distribution for coagulation by Brownian motion. *J. Colloid Inter. Sci.* **22,** 126.
Friedlander, S. K. (1977) *Smoke, Dust and Haze.* Wiley–Interscience, New York.
Fuchs, N. A. (1964) *Mechanics of Aerosols.* Pergamon, New York.
Fuchs, N. A. and Sutugin, A. G. (1965) Coagulation rate of highly dispersed aerosols. *J. Colloid Sci.* **20,** 492.
Gangopadhyay, S., Elminyawi, I. and Sorensen, C. M. (1991) Optical structure factor measurements of soot particles in a premixed flame. *Appl. Opt.* **30,** 4859.
Jander, H., Petereit, N. and Razus, D. M. (1995) The influence of carbon density on soot growth in atmospheric C_2H_4 (air, O_2) flames. *Z. Phys. Chemie* **188,** 159.
Kerker, M. (1969) *The Scattering of Light and Other Electromagnetic Radiation.* Academic Press, New York.
Kim, C. S. and Liu, B. Y. H. (1984) *Aerosols* (Edited by Liu, B. Y. H., Pui, D. Y. and Fissan, H. J.), p. 923. Elsevier, New York.
Koylu, U. O. and Faeth, G. M. (1992) Structure of overfire soot in bouyant diffusion turbulent flames at long residence times. *Combust. Flame* **89,** 140.
Koylu, U. O. and Faeth, G. M. (1996) Spectra extinction coefficients of soot aggregate from turbulent diffusion flames. *J. Heat Trans.* **118,** 415.
Lai, F. S., Friedlander, S. K., Pich, J. and Hidy, G. M. (1972) The self-preserving particle size distribution for Brownian coagulation in the free-molecule regime. *J. Colloid Inter. Sci.* **39,** 395.
Marlow, W. H. (1980a) Derivation of aerosol collision rates for singular attractive contact potentials. *J. Chem. Phys.* **73,** 6284.
Marlow, W. H. (1980b) Lifshitz-van der Waals forces in aerosol particle collisions—I. Introduction: water droplets. *J. Chem. Phys.* **73,** 6288.
Marlow, W. H. (1981) Size effects in aerosol particle interactions: the van der Waals potential and collision rates. *Surf. Sci.* **106,** 529.
Martin, J. E. and Schaefer, D. W. (1984) Dynamics of fractal colloidal aggregates. *Phys. Rev. Lett.* **53,** 2457.
Meakin, P., Chen, Z.-Y. and Deutch, J. M. (1985) The translational friction coefficient and time dependent cluster size distribution of three dimensional cluster–cluster aggregation. *J. Chem. Phys.* **82,** 3786.
Meakin, P., Donn, B. and Mulholland, G. W. (1989) Collisions between point masses and fractal aggregates. *Langmuir* **5,** 510.
Mercer, T. T. (1976) *Fundamentals of Aerosol Science* (edited by Shaw, D. T.) p. 85. Wiley, New York.
Mulholland, G. W., Samson, R. J., Mountain, R. D. and Ernst, M. H. (1988) Cluster size distribution for free molecular agglomeration. *J. Energy Fuels* **2,** 481.
Oh, C. and Sorensen, C.M. (1997) J. Colloid Inter. Sci., submitted.
Okuyama, K., Kousaka, Y. and Hayashi, K. (1984) Change in size distribution of ultrafine aerosol particles undergoing Brownian coagulation. *J. Colloid Inter. Sci.* **101,** 98.
Okuyama, K., Kousaka, Y. and Hayashi, K. (1986) Brownian coagulation of two-component ultrafine aerosols. *J. Colloid Inter. Sci.* **113,** 42.
Olivier, B. J. and Sorensen, C. M. (1990) Aggregation kernel homogeneity dependence on aggregant concentration in gold colloids. *Phys. Rev. A* **41,** 2093.
Olivier, B. J., Sorensen, C. M. and Taylor, T. W. (1992) Scaling dynamics of aerosol coagulation. *Phys. Rev. A* **45,** 5614.
Prado, G., Jagoda, J., Neoh, K. and Lahaye, J. (1981) A study of soot formation in premixed propane/oxygen flames by in-situ optical techniques and sampling probes. *Proc. 18th Int. Symp.* on Combustion. The Combustion Institute, Pittsburgh, PA.
Puri, R., Richardson, T. F., Santoro, R. J. and Dobbins, R. A. (1993) Aerosol dynamic processes of soot aggregates in a laminar ethene diffusion flame. *Combust. Flame* **92,** 320.
Pusey, P. N., Rarity, J. G., Klein, R. and Weitz, D. A. (1987) Comment on "hydrodynamic behavior of fractal aggregates". *Phys. Rev. Lett.* **59,** 2122.

Rogak, S. N. and Flagan, R. C. (1992) Coagulation of aerosol agglomerates in the transition regime. *J. Colloid Inter. Sci.* **151,** 203.
Samson, R. J., Mulholland, G. W. and Gentry, J. W. (1987) Structural analysis of soot agglomerates. *Langmuir* **3,** 273.
Schaefer, D. W., Martin, J. E., Wiltzius, P. and Cannell, D. S. (1984) Fractal geometry of colloidal aggregates. *Phys. Rev. Lett.* **52,** 2371.
Seinfeld, J. H., (1986) *Atmospheric Chemistry and Physics of Air Pollution.* Wiley, New York.
Sorensen, C. M., (1997) *Scattering and Absorption of Light by Particles and Aggregates.* CRC Press.
Sorensen, C. M. and Roberts, G. C. (1997) The prefactor of fractal aggregates. *J. Colloid Inter. Sci.* (submitted).
Sorensen, C. M., Cai, J., and Lu, N. (1992a) Light-scattering measurements of monomer size, monomers per aggregate, and fractal dimension for soot aggregates in flames. *Appl. Opt.* **31,** 6547.
Sorensen, C. M., Cai, J., and Lu, N. (1992b) Test of static structure factors for describing light scattering from fractal soot aggregates. *Langmuir* **8,** 2064.
Szymanski, W. W., Majerowicz, A. and Wagner, P. E. (1989) Measurement of Brownian coagulation in monodispersed and bidispersed liquid aerosols. *Aerosol Sci. Technol.* **11,** 1.
Vaglieco, B. M., Beretta, F. and D'Alessio, A. (1990) In situ evaluation of the soot refractive index in the UV-visible from the measurement of the scattering and extinction coefficients in rich flames. *Combust. Flame* **79,** 259.
van Dongen, P. G. J. and Ernst, M. H. (1985) Dynamic scaling in kinetics of clustering. *Phys. Rev. Lett.* **54,** 1396.
Wagner, P. E. and Kerker, M. (1977) Brownian coagulation of aerosols in rarefied gases. *J. Chem. Phys.* **66,** 638.
Weitz, D. A. and Oliveria, M. (1984) Fractal structures formed by kinetic aggregation of aqueous gold colloids. *Phys. Rev. Lett.* **52,** 1433.
Weitz, D. A., Huang, J. S., Lin, M. Y. and Sung, J. (1984) Dynamics of diffusion-limited kinetic aggregates. *Phys. Rev. Lett.* **53,** 1657.
Wiltzius, P. (1987) Hydrodynamic behavior of fractal aggregates. *Phys. Rev. Lett.* **58,** 710.
Wiltzius, P. and van Saarloos, W. (1987) Wiltzius and van Saarloos reply. *Phys. Rev. Lett.* **59,** 2123.
Wu, M. K. and Friedlander, S. K. (1993) Enhanced power law agglomerate growth in the free molecular regime. *J. Aerosol Sci.* **24,** 273.
Zhang, H. X., Sorensen, C. M., Ramer, E. R., Olivier, B. J. and Merklin, J. F. (1988) In situ optical structure factor measurements of an aggregating soot aerosol. *Langmuir* **4,** 867.

APPENDIX A

The large size limit of the scaling distribution is

$$n(v, t) = M_1 s_p^{-2} \phi(x), \tag{A1}$$

with normalized size

$$x = v/s_p, \tag{A2}$$

mean size

$$s_p(t) = M_p/M_{p-1}, \tag{A3}$$

and moments

$$M_i(t) = \int_0^\infty v^i n(v, t)\, dv. \tag{A4}$$

The reduced size distribution or scaling function is

$$\phi(x) = A x^{-\lambda} e^{-\alpha x} \tag{A5}$$

where λ is the kernel homogeneity (Class II kernels) and A and α are constants determined below.

Substitute equations (A1) and (A2) into equation (A4) to find

$$M_i = M_1 s_p^{i-1} m_i \tag{A6}$$

where m is the ith moment of the scaling function

$$m_i = \int x^i \phi(x)\, dx. \tag{A7}$$

Subsitute equation (A5) into equation (A7) to find

$$m_i = A\alpha^{\lambda-i-1}\, \Gamma(i + 1 - \lambda) \tag{A8}$$

where $\Gamma(x)$ is the Gamma function.

The choice of the mean size s_p is arbitrary and hence can be made in accord with experimental convenience. Once a value of p is chosen for s_p, the value of α in equation (A5) is determined as follows. Substitute equation (A6) into equation (A3) to find

$$m_p = m_{p-1} \tag{A9}$$

when the mean size is defined as s_p. Use equation (A8) in equation (A9) to find

$$\alpha = p - \lambda. \tag{A10}$$

The constant A is found from the normalization condition for the size distribution to the total mass (or volume or number of monomers) M_1. For $i = 1$, equation (A6) yields

$$m_1 = 1. \tag{A11}$$

From this and equation (A8) one obtains

$$A = \alpha^{2-\lambda}/\Gamma(2 - \lambda). \tag{A12}$$

Next we find a relationship between the various mean sizes. Consider the ratio s_{i+1}/s_i. From equations (A3), (A6) and (A7) this equals $m_{i+1} m_{i-1} m_i^{-2}$. Then equation (A8) yields $(i + 1 - \lambda)/(i - \lambda)$ which leads to

$$s_n = s_1 \frac{n - \lambda}{1 - \lambda}. \tag{A13}$$

In summary, the scaling distribution is given by equations (A1), (A2) and (A5). The constant α and A in equation (A5) are determined by the choice of which mean size to use in equation (A1), i.e. what value of p, and normalization to the total mass, and are given by equations (A10) and (A12), respectively. We conclude with two simple cases, both of which have $\lambda = 0$.

If $p = 1$,

$$\alpha = 1, \qquad A = 1, \quad s_n = n s_1.$$

If $p = 2$,

$$\alpha = 2, \qquad A = 4, \qquad s_n = n s_1.$$

APPENDIX B

The ith moment of the cluster size distribution evolving in accord with the Smoluchowski equation has a time derivative given by

$$\dot{M}_i(t) = \frac{1}{2} \int_0^\infty \int_0^\infty [(v + u)^i - v^i - u^i] \, K(v, u) \, n(v, t) \, n(u, t) \, dv \, du. \tag{B1}$$

Now substituting the scaling form for the size distributions with $x = v/s$ and $y = u/s$ and by taking advantage of the homogeneity of the kernel we obtain

$$\dot{M}_i(t) = s^{i+\lambda-2} \, M_1^2 \, I_i, \tag{B2}$$

where we define

$$I_i = \frac{1}{2} \int_0^\infty \int_0^\infty [(x + y)^i - x^i - y^i] \, K(x, y) \, \phi(x) \, \phi(y) \, dx \, dy. \tag{B3}$$

For reasons described below it is useful to modify equation (B2) by multiplying it by $s^{-\lambda} K(s, s)/K(1, 1)$ which equals unity to obtain (for the moment we leave the mean size arbitrary with no subscript p)

$$\dot{M}_i(t) = s^{i-2} \, M_1^2 \, P_i \, K(s, s) \tag{B4}$$

where

$$P_i = I_i/K(1, 1). \tag{B5}$$

Comparison of equation (B3) with equation (B5) shows that the material dependent parameters in the aggregation kernel cancel in equation (B5) so that P_i is dependent only on the functional form of $K(x, y)$. Now consider two special cases.

Case $i = 0$: When $i = 0$, equation (B4) becomes

$$\dot{M}_0(t) = s^{-2} M_1^2 P_0 K(s, s). \tag{B6}$$

Now recognize that the average number of clusters is the total number of monomers (or total mass or total volume) divided by the mean cluster size (in terms of monomers, mass or volume). Since there are an infinite number of ways to define the average size, $s_p = M_p/M_{p-1}$, there are an infinite number of cluster number densities

$$n_p = M_1/s_p. \tag{B7}$$

If we pick $p = 1$ to define the mean size, $s_1 = M_1/M_0$, then the cluster number density is simply

$$n_1 = M_0. \tag{B8}$$

Then equation (B6) can be written as

$$\dot{n}_1(t) = n_1^2 P_0 K(s_1, s_1). \tag{B9}$$

Note that $P_0 < 0$ which ensures the monotonic decrease of $n_1(t)$ through aggregation. The value of equation (B9) is that it has the same form as the simple approximation to the Smoluchowski equation made under the assumption of a constant kernel and a monodisperse size distribution. Then

$$\dot{n} = -\tfrac{1}{2} K n^2, \tag{B10}$$

where K is the aggregation constant. The often found usefulness of the simple equation (B10) is due to its similarity to the exact result of equation (B9). If the kernel homogeneity is zero, $K(s_0, s_0)$ is a constant equal to K. The factor P_0 is a *polydispersity factor* with absolute value equal to 0.5 for a monodisperse cluster distribution, but in general $|P_0| \geqslant 0.5$. If the kernel homogeneity is not zero, then K is not constant, but for small intervals of s (or n) equation (B9) implies that equation (B10) would still be a useful approximation.

Case $i = 2$: When $i = 2$, equation (B4) becomes

$$\dot{M}_2(t) = M_1^2 P_2 K(s, s). \tag{B11}$$

This situation applies to light scattering measurements because at small angles the scattering per cluster is proportional to the square of the number of monomers per cluster. Hence we pick for the mean size in the scaling equation $s_2 = M_2/M_1$. By equation (B7) $n_2 = M_1/s_2 = M_1^2/M_2$. The time derivative of n_2 is

$$\dot{n}_2 = -M_1^2/M_2^2 \dot{M}_2 \tag{B12}$$

$$= -n_2^2 P_2 K(s_2, s_2). \tag{B13}$$

Once again we have an exact result (B13) similar to the simple Smoluchowski equation (B10). The factor $P_2 \geqslant 1$ is the appropriate polydispersity factor when mean size and cluster number density are defined by $p = 2$.

In this work n_2 is measured directly with light scattering. P_2 must be calculated using an assumed functional form for the kernel. One does not need the magnitude of the kernel for this calculation; it is this magnitude we aspire to measure experimentally. Measurement of n_2 and s_2 and calculation of P_2 allows the kernel $K(s_2, s_2)$ to be measured as a function of s_2.

The values of P_0 and P_2 were calculated numerically for the three regimes continuum, Epstein and free molecular using equations (B3) and (B5). To find the size distribution $n(u, t)$ and hence the scaling function $\phi(s)$, the Smoluchowski equation was solved using a fourth-order Runge–Kutta method using the aggregation kernels given in Table 1 until scaling was achieved. The results are given in Table B1.

Table B1. Polydispersity factors for the three limiting aggregation regimes.

Polydispersity factor	Continuum	Epstein	Free molecular
P_0	−0.59	−0.73	−0.67
P_2	1.10	1.36	1.14